

EDS results, $M_{23}C_6$ (Cr-rich) precipitates were observed, while MX precipitates were too small to be observed [6].

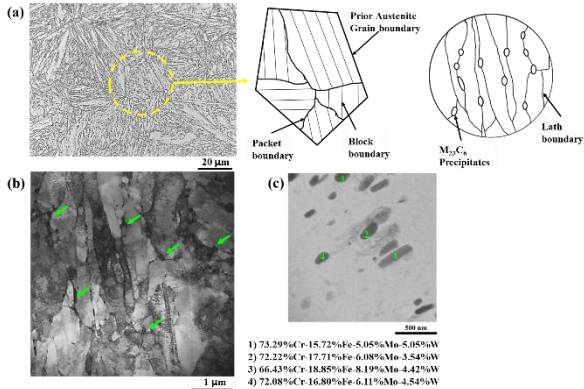


Figure 1. The cross-sectional (a) OM and (b), (c) TEM micrograph of the initial HT9 cladding with tempered martenite microstructure and $M_{23}C_6$ precipitate at lath boundaries.

2.2 Thermal Creep measurement.

Thermal creep tests were conducted considering the operating conditions of SFRs and SMFRs at effective stresses of 17–120MPa and temperatures of 873–923 K. The preparation and measurement of thermal creep tests referred to ASTM E139 and E8/E8M standards [7–8]. The HT9 cladding were enclosed at both ends with end caps made of the HT9, with one end cap equipped with a passage for pressure gas. A pressurization welding system capable of injecting pressure and arc welding was manufactured to fabricate the thermal creep specimens. The specimens were inserted into the pressurization welding system, and the internal chamber was evacuated to 1×10^{-3} torr before injecting argon, Ar gas up to the test pressure. After maintaining pressure for 30 minutes to ensure sufficient injection, the gas injection port was arc-welded to seal the specimen. The weight of the fabricated specimens was measured before and after fabrication, and the injection pressure was calculated using the ideal gas equation. For thermal creep testing, the specimens were sealed in vacuum quartz along with tantalum, Ta foil for oxidation protection and heat-treated in furnace. Every 1,000-h, the specimens were removed from furnace and measured the outer diameter using a laser diameter measurement system, rotating the specimen 360° and measuring at 5mm intervals along the length direction. The stress was calculated as the circumferential stress and Von Mises equation [9] to determine the effective stress, and the diameter strain obtained from the test was converted to effective stress considering mid-wall strain [10].

Fig. 2 presented thermal creep strain curves obtained from the thermal creep tests up to 20,000-h within the stress range of 17–120MPa at three temperatures (873, 893, and 923K). Generally, creep strain curves exhibit three distinct regimes over time: primary (transient), secondary (steady-state), and tertiary (acceleration), with some conditions transitioning from the primary to

tertiary regime [11]. Furthermore, both creep strain and creep rate increase with increasing temperature and stress. In this study, most conditions significantly showed primary and secondary regimes in the creep tests, with some specimens experiencing tertiary creep and rupture at high stress levels at each temperature. The minimum strain for rupture occurred when the strain exceeded 1%. The conditions of 102 MPa–873 K, and 68MPa–893K are representative examples. Since strain measurements were conducted every 1,000-h, the primary creep regime could not be distinctly identified, however, due to the clear representation of secondary creep strain curves, the creep stages were determined focusing on secondary creep. Primary creep is characterized by a linear increase in the secondary creep strain curve, indicating a constant creep rate. For instance, in Fig. 3, the segment where the creep rate remains constant in both the creep strain curve (see Fig 3(a)) and creep rate curve (see Fig 3(b)) is determined as the secondary creep regime. For example, at 81 MPa–873 K, the secondary creep rate is maintained at 5.4×10^{-5} %/h. By representing this segment as a linear line on the creep strain curve, the primary creep deformation rate can be calculated. Tertiary creep is characterized by a rapid increase in strain, but the selection of segments was challenging due to the 1,000-h measurement interval.

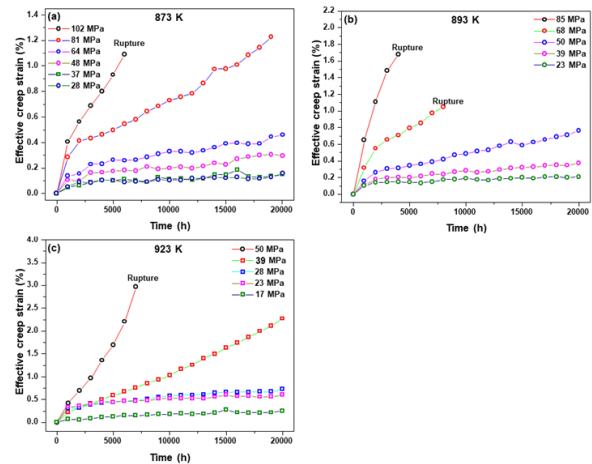


Figure 2. Experimentally obtained thermal creep strain curves of manufactured HT9 cladding in the stress ranges of 10–120 MPa at (a) 873 K, (b) 893 K, and (c) 923 K.

2.3 Thermal creep correlations

In evaluating the thermal creep properties of the manufactured HT9 cladding by KAERI, it is essential to compare them with reported creep prediction correlations. Widely used creep correlations include Norton's power law [12], the theta projection [13], and Garofalo's equation [14]. The theta projection was developed by Evans [13], and Lewis and Chung [15] developed the creep correlation for HT9. This correlation is based on the parameters of primary and tertiary creep; however, since the creep strain obtained in this study primarily exhibits secondary creep over a long duration,

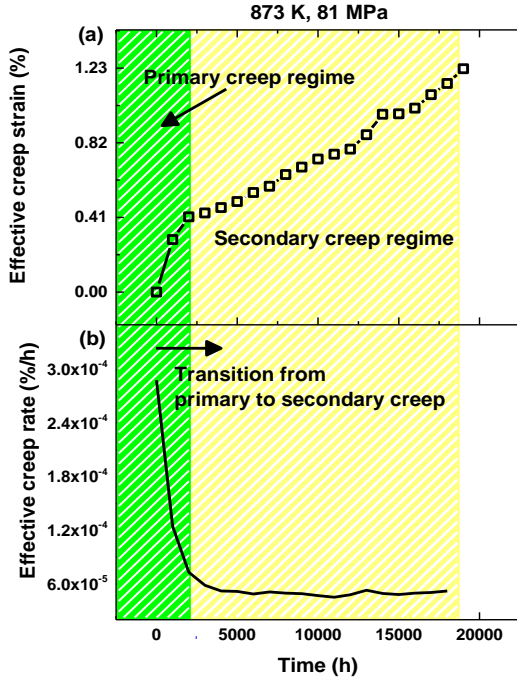


Figure 3. (a) Thermal creep strain and (b) creep rate curves of manufactured HT9 cladding up to 20,000-h at 81 MPa and 873 K showing the classification of primary and secondary creep regimes.

it is not suitable. Therefore, comparison was made with modified Garofalo's equation [16], which includes Norton's power law [12], Arrhenius equation [17], and Garofalo's equation [14]. The modified Garofalo's equation [16] is the following equation, where the primary strain is composed of a power law and exponential function. The stress exponent, denoted as n , represents the creep mechanism, where values below 2 indicate diffusion creep and values above 2 indicate dislocation creep [18].

$$\varepsilon_T = \varepsilon_p + \varepsilon_s + \varepsilon_t \quad (1)$$

$$\varepsilon_p = \left[C_1 \exp\left(\frac{-Q_1}{RT}\right) \cdot \sigma^{n_1} + C_2 \exp\left(\frac{-Q_2}{RT}\right) \sigma^{n_2} + C_3 \exp\left(\frac{-Q_3}{RT}\right) \cdot \sigma^{n_3} \right] \cdot [1 - \exp(-C_4 t)] \quad (2)$$

$$\varepsilon_s = (C_5 \exp\left(\frac{-Q_4}{RT}\right) \sigma^{n_3} + C_6 \exp\left(\frac{-Q_5}{RT}\right) \sigma^{n_5}) \cdot t \quad (3)$$

$$\varepsilon_t = C_7 \exp\left(\frac{-Q_6}{RT}\right) \sigma^{n_6} t^{n_7} \quad (4)$$

where ε_T , ε_p , ε_s , and ε_t are total, primary, secondary, and tertiary creep strains, respectively. C , Q , R , T , σ and n are material constant, activation energy, gas constant, temperature, effective stress, and exponent of stress and time, respectively.

Fig. 4 shows comparison between the modified Garofalo's equation [16] and the experimentally obtained thermal creep strain at 873K. Although the creep behavior is similar, there are differences in strain with respect to stress. To predict the thermal creep behavior of manufactured HT9 cladding, a new creep prediction correlation was derived utilizing this equation. Based on the creep rate, when plotted on a log-form graph as shown in Fig. 5(a) and (b), the creep rates and stresses of

primary and secondary creep can be represented as linear lines. For primary creep, n took values of 1 and 2, while for secondary creep, it takes values of 2 and 4. Material constants C and activation energy Q can be derived from the linear function of the log-form creep rate and reciprocal temperature graph in Fig 5(c) and (d). Garofalo's equation [14], as a function of time for primary creep, represents the transition from primary to secondary creep, with the material constant C_4 calculated from the time it takes for the transition from primary to secondary creep. For the tertiary creep correlation, due to the limited number of specimens showing tertiary creep in this study and the error introduced by the 1,000-h measurement interval, it was difficult to derive. A new creep correlation derived in this study including primary and secondary creep equation is as follows:

$$\varepsilon_p = (1.55 \cdot 10^4 \exp\left(\frac{-27792}{RT}\right) \sigma^{0.95} + 3.68 \cdot 10^6 \exp\left(\frac{-45241}{RT}\right) \sigma^{2.04}) \cdot (1 - \exp(-4 \cdot 10^{-7} \cdot t)) \quad (5)$$

$$\varepsilon_s = (1.15 \cdot 10^5 \exp\left(\frac{-70582}{RT}\right) \sigma^{2.10} + 8.12 \cdot 10^{12} \exp\left(\frac{-116669}{RT}\right) \sigma^{4.40}) \cdot t \quad (6)$$

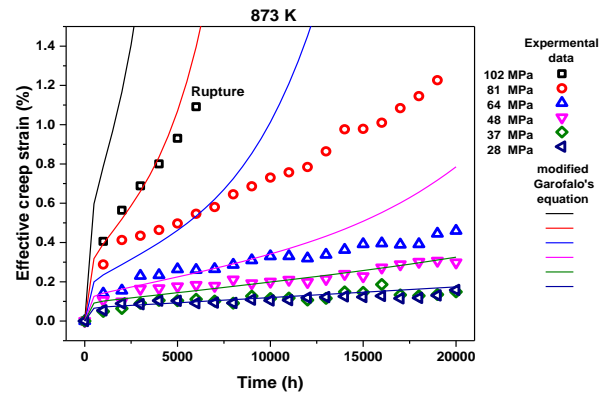


Figure 4. Comparison between modified Garofalo's equation [16] and experimentally obtained thermal creep strains at 873 K.

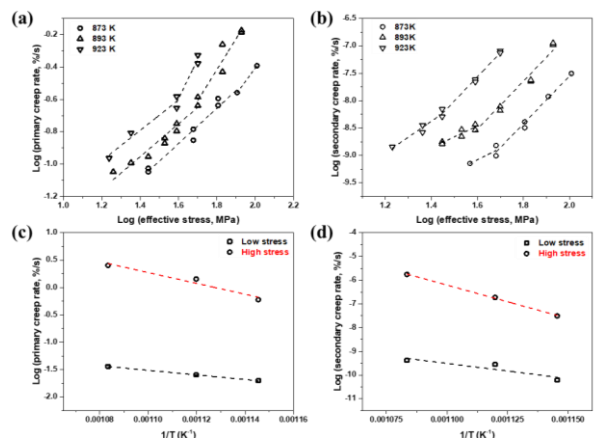


Figure 5. Log-forms of primary and secondary creep rate as function of a log-form of effective stress and reciprocal temperature. Curves to derive the stress exponent, n of (a) primary and (b) secondary creep, and derive the constants including activation, Q of (c) primary and (d) secondary creep.

REFERENCES

Fig. 6 presents the newly derived creep correlation with experimentally obtained thermal creep strains. The discrepancies observed at 923 K is attributed to the absence of tertiary creep. However, most of the derived creep correlation matches well the thermal creep strains.

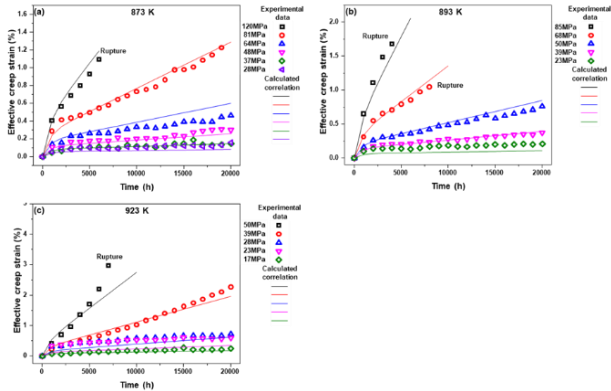


Figure 6. Comparison of the developed creep correlation and experimentally obtained thermal creep strains of manufactured HT9 cladding as function of the time at stress and temperature ranges of 17–120 MPa and 873–923 K, respectively.

3. Conclusions

The research team at KAERI successfully manufactured HT9 cladding, candidate materials for SFRs and SMFRs, through cold working, hot working, and heat treatment processes. The microstructure of the manufactured HT9 consists of typical tempered martensite, with $M_{23}C_6$ precipitates also observed at the interfaces. Creep strength is a key factor in determining the mechanical properties and life-time of nuclear fuel cladding. Therefore, thermal creep tests were conducted based on various operating conditions ranging from 17–120MPa and 873–923K for advanced reactor. To perform thermal creep tests, a pressurization welding system for manufacturing thermal creep specimens and a laser diameter measurement system for measuring diameter changes were designed. Thermal creep strain curves up to 20,000-h primarily showed primary and secondary creep regimes, with tertiary creep and rupture occurring at some high stresses. To compare creep strength and develop a creep prediction correlation, experimentally obtained thermal creep strains were compared with creep prediction correlations. Predicting the creep strain of the manufactured HT9 cladding difficult from reported creep correlations, thus a new correlation based on the modified Garofalo's equation [16] was derived. Due to the absence of tertiary creep and rupture time data, a tertiary creep correlation could not be derived. However, the newly derived correlation matches well with the experimental data. Future works involve minimizing errors in creep strain curves by shortening the measurement interval using in-situ creep strain measurement equipment and developing tertiary creep and rupture correlations

- [1] X. Ren, K. Sridharan, T. Allen, Corrosion of ferritic–martensitic steel HT9 in supercritical water, *Journal of Nuclear Material*, vol. 358, p227, 2006.
- [2]R. Klueh, A.T. Nelson, Ferritic/martensitic steels for next-generation reactors, *Journal of Nuclear Materials*. Vol. 371 p. 37, 2007.
- [3]D. S. Gelles, Microstructural examination of commercial ferritic alloys at 200 dap, *Journal of Nuclear materials*, Vol. 233, p. 293, 1996.
- [4] M. Rolinska, F. Gustavsson, P. Hedstrom, Revisiting the applications of the extraction replica sample preparation technique for analysis of precipitates in engineering alloys, *Materials Characterization*, Vol. 198, p. 111978, 2022.
- [5]J. Hald, Microstructure and long-term creep properties of 9–12% Cr steels, *International Journal of Pressure Vessel and Piping*, Vol. 85, p. 30, 2008.
- [6]C. Zheng, M.A. Auger, M.P. Moody, D. Kaoumi, Radiation induced segregation and precipitation behavior in self-ion irradiated Ferritic/Martensitic HT9 steel, *Journal of Nuclear Materials*, Vol. 491, p. 162, 2017.
- [7]ASTM, E139-11, "Standard test methods for conducting creep, creep-rupture, and stress rupture tests of metallic materials." 2018.
- [8]ASTM, E8/E8M-08, "Standard test methods for tension testing of metallic materials." West Conshohocken, PA 3, 2016.
- [9]H.J. Ryu, Y.S. Kim, A. Yacout, Thermal creep modeling of HT9 steel for fast reactor applications, *Journal of Nuclear Materials*, Vol. 409, p. 207, 2011.
- [10]M. Toloczko, B. Grambau, F. Garner, K. Abe, Comparison of Thermal Creep and Irradiation Creep of HT9 Pressurized Tubes at Test Temperatures from $\sim 490^\circ\text{C}$ to 605°C , *Effects of Radiation on Materials: 20th International Symposium*, ASTM International, 2001.
- [11]F. Abe, T. Kern and R. Viswanathan, *Creep-resistant steels*, Woodhead publishing limited, p4.
- [12]F.H. Norton, *The creep of steel at high temperatures*, McGraw-Hill, New York, 1929.
- [13]R. Evans, J. Parker, B. Wilshire, The θ projection concept—A model-based approach to design and life extension of engineering plant, *International Journal of Pressure Vessel and Piping*, Vol. 50, p. 147, 1992.
- [14]F. Garofalo, D.B. Butrymowicz, *Fundamentals of creep and creep-rupture in metals*, Macmillan, New York, 1965.
- [15]G. Lewis, C.-C. Chuang, Constitutive thermal creep deformation relations for lifetime prediction of a fusion reactor first wall ferritic alloy, *Fusion Engineering Design*, Vol. 13, p.407, 1991.
- [16] L.L. Briggs, Y.I. Chang, D. Hill, J. Ahrens, M. Billone, D. Crawford, E. Filewicz, P. Finck, E. Fujita, K. Grimm, *Safety Analysis and Technical Basis for Establishing an Interim Burnup Limit for Mark-V and Mark-VA Fuel Subassemblies in EBR-II*, Argonne National Lab.(ANL), Argonne, ILUnited States, 2018.
- [17]X. Niu, L. Shen, C. Chen, J. Zhou, L. Chen, An Arrhenius-type constitutive model to predict the deformation behavior of Sn0.3Ag0.7Cu under different temperature, *Journal of Materials Science: Materials in Electronics*, Vo. 30, p.14611, 2019.
- [18]V. Sklenička, K. Kuchařová, M. Svoboda, L. Kloc, Burší, x, J. k, A. Kroupa, Long-term creep behavior of 9–12%Cr power plant steels, *Materials Characterization*, Vol. 51, p. 35, 2003.